ISSN 1674-1056
http://cpb.iphy.ac.cn
http://iopscience.iop.org/cpb
中国物理 B
Chinese Physics
中国物理 Chinese Physics B

Particle-hole fluctuations and possible superconductivity in doped α-$RuCl_3$

Bin-Bin Wang(王斌斌), Wei Wang(王巍), Shun-Li Yu(于顺利), Jian-Xin Li(李建新)

Citation: Chin. Phys. B . 2019, 28(5): 057402. **doi:** 10.1088/1674-1056/28/5/057402
Journal homepage: http://cpb.iphy.ac.cn; http://iopscience.iop.org/cpb

What follows is a list of articles you may be interested in

High-throughput research on superconductivity

Mingyang Qin(秦明阳), Zefeng Lin(林泽丰), Zhongxu Wei(魏忠旭), Beiyi Zhu(朱北沂), Jie Yuan(袁洁), Ichiro Takeuchi, Kui Jin(金魁)
Chin. Phys. B . 2018, 27(12): 127402. **doi:** 10.1088/1674-1056/27/12/127402

A single-crystal neutron diffraction study on magnetic structure of $CsCo_2Se_2$

Juanjuan Liu(刘娟娟), Jieming Sheng(盛洁明), Wei Luo(罗伟), Jinchen Wang(汪晋辰), Wei Bao(鲍威), Jinhu Yang(杨金虎), Minghu Fang(方明虎), S A Danilkin
Chin. Phys. B . 2018, 27(11): 117401. **doi:** 10.1088/1674-1056/27/11/117401

Superconductivity with peculiar upper critical fields in quasi-one-dimensional Cr-based pnictides

Guang-Han Cao(曹光旱), Zeng-Wei Zhu(朱增伟)
Chin. Phys. B . 2018, 27(10): 107401. **doi:** 10.1088/1674-1056/27/10/107401

Advanced high-pressure transport measurement system integrated with low temperature and magnetic field

Jing Guo(郭静), Qi Wu(吴奇), Liling Sun(孙力玲)
Chin. Phys. B . 2018, 27(7): 077402. **doi:** 10.1088/1674-1056/27/7/077402

Nodeless superconductivity in a quasi-two-dimensional superconductor $AuTe_2Se_{4/3}$

Xiao-Yu Jia(贾小雨), Yun-Jie Yu(俞云杰), Xu Chen(陈旭), Jian-Gang Guo(郭建刚), Tian-Ping Ying(应天平), Lan-Po He(何兰坡), Xiao-Long Chen(陈小龙), Shi-Yan Li(李世燕)
Chin. Phys. B . 2018, 27(6): 067401. **doi:** 10.1088/1674-1056/27/6/067401

Particle–hole fluctuations and possible superconductivity in doped α-$RuCl_3$*

Bin-Bin Wang(王斌斌)[1], Wei Wang(王巍)[1], Shun-Li Yu(于顺利)[1,2,†], and Jian-Xin Li(李建新)[1,2,‡]

[1] *National Laboratory of Solid State Microstructures and Department of Physics, Nanjing University, Nanjing* 210093, *China*
[2] *Collaborative Innovation Center of Advanced Microstructures, Nanjing University, Nanjing* 210093, *China*

(Received 30 January 2019; revised manuscript received 19 March 2019; published online 4 April 2019)

We study various particle–hole excitations and possible superconducting pairings mediated by these fluctuations in doped α-$RuCl_3$ by using multi-band Hubbard model with all t_{2g} orbitals. By performing a random-phase-approximation (RPA) analysis, we find that among all particle–hole excitations, the $j_{\rm eff} = 1/2$ pseudospin fluctuations are dominant, suggesting the robustness of $j_{\rm eff} = 1/2$ picture even in the doped systems. We also find that the most favorable superconducting state has a d-wave pairing symmetry.

Keywords: superconductivity, particle–hole fluctuations, spin–orbit coupling, α-$RuCl_3$

PACS: 74.20.Rp, 75.10.Lp, 71.70.Ej, 71.10.Fd **DOI:** 10.1088/1674-1056/28/5/057402

1. Introduction

The doped Mott insulators[1–6] have been subject to extensive investigations because they contain plentiful phases, such as spin-density wave (SDW), pseudogaps, and superconductivity. In parent compounds, the charge insulation of most Mott insulators raises solely from the Coulomb interaction. However, recently a new family of Mott insulator, in which the charge insulation is resulted from the cooperative interplay between spin–orbit coupling (SOC) and electron correlation, has been proposed, such as Sr_2IrO_4,[7,8] Na_2IrO_3,[9–11] and α-$RuCl_3$.[12–14] In these Mott insulators, the electron configuration for the active ions is d^5, such as $5d^5$ of Ir^{4+} in iridates and $4d^5$ of Ru^{3+} in ruthenium. Within the octahedral crystal field, the d orbitals are split into a two-fold e_g manifold and a three-fold t_{2g} manifold with an effective $l_{\rm eff} = 1$ orbital moment. The latter are further divided into a fully filled $j_{\rm eff} = 3/2$ band and a half-filed $j_{\rm eff} = 1/2$ narrow band by strong SOC. Then the $j_{\rm eff} = 1/2$ band only needs a moderate electronic correlation to open a Mott gap. Thus these Mott insulators are usually referred to as spin–orbit assisted Mott insulators.

The novel physics of these $j_{\rm eff} = 1/2$ Mott materials in different lattices has been reported both experimentally and theoretically. For the square lattice, a canted antiferromagnetic structure has been found in Sr_2IrO_4,[15–17] which is isostructural to La_2CuO_4, a parent compound for cuprate superconductors. Similar to the doped cuprate Mott insulator, pseudogap, Fermi arc,[18–21] and superconductivity[22–26] are also addressed in doped Sr_2IrO_4. For the honeycomb lattice, an intriguing physics is that the Kitaev interactions underlying the celebrated Kitaev model,[27] whose ground state is exactly a Z_2 spin liquid with Majorana fermion excitations, can be realized.[28] In this aspect, the honeycomb-lattice material α-$RuCl_3$ has recently attracted much attention.[12–14,29,30] Although the ground state of α-$RuCl_3$ has a long-range zigzag magnetic order, a broad continuous spectrum in inelastic neutron scattering has been observed[12–14] and the magnetic order can be fully suppressed by either an in-plane magnetic field[31–33] or pressure.[34–36] There is accumulating evidence that the field-induced disordered state is a promising candidate as a quantum spin liquid.[31–33] For doped systems, the $j_{\rm eff} = 1/2$ Mott materials with honeycomb lattice also exhibit many exotic physics, such as unconventional superconductivity[37–41] and unique charge dynamics.[42–49]

In this paper, based on the multi-band Hubbard model including all t_{2g} orbitals, we investigate various particle–hole (PH) excitations and possible superconducting pairings mediated by these fluctuations in the doped systems with the random-phase-approximation (RPA) method. We find that the $j_{\rm eff} = 1/2$ pseudospin fluctuations dominate over the fluctuations from other particle–hole excitations, suggesting the robustness of the $j_{\rm eff} = 1/2$ picture even in the doped systems, and the most favorable superconducting state mediated by the pseudospin fluctuations has a d-wave pairing symmetry.

2. Method

The low-energy physics of α-$RuCl_3$ is dominated by the t_{2g} orbitals due to the $4d^5$ configuration of Ru^{3+} and the octahedral crystal field, so our calculations are based on the t_{2g}

*Project supported by the National Natural Science Foundation of China (Grant Nos. 11674158 and 11774152) and the National Key Projects for Research and Development of China (Grant No. 2016YFA0300401). W. Wang was also supported by the Program B for Outstanding PhD Candidate of Nanjing University.

†Corresponding author. E-mail: slyu@nju.edu.cn
‡Corresponding author. E-mail: jxli@nju.edu.cn

© 2019 Chinese Physical Society and IOP Publishing Ltd

three-orbital model,[30] which is derived through fitting the band structure from the density-functional theory (DFT). The three-orbital Hamiltonian is given as

$$H = H_{t_{2g}} + H_{soc} + H_{int}, \tag{1}$$

where the parameters in the three-orbital tight-binding Hamiltonian $H_{t_{2g}}$ and SOC H_{soc} are from Ref. [30]. The band structure of this three-orbital model with SOC is shown in Fig. 1. The interactions between electrons are included in H_{int} as follows:

$$\begin{aligned} H_{int} = & U\sum_{i\mu} n_{i\mu\uparrow}n_{i\mu\downarrow} + U'\sum_{i,\mu<\nu}\sum_{\sigma\sigma'} n_{i\mu\sigma}n_{i\nu\sigma'} \\ & + J_h\sum_{i,\mu<\nu}\sum_{\sigma\sigma'} d^\dagger_{i\mu\sigma}d^\dagger_{i\nu\sigma'}d_{i\mu\sigma'}d_{i\nu\sigma} \\ & + J'\sum_{i,\mu\neq\nu} d^\dagger_{i\mu\uparrow}d^\dagger_{i\mu\downarrow}d_{i\nu\downarrow}d_{i\nu\uparrow}, \end{aligned} \tag{2}$$

where U (U') is the intra-orbital (inter-orbital) Coulomb interaction, J_h and J' are the Hund's coupling and pair hopping, respectively. In this paper, we employ $U = U' + 2J_h$ and $J_h = J'$.

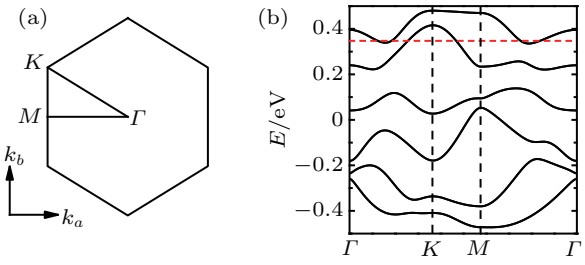


Fig. 1. (a) Brillouin zone of the honeycomb lattice. (b) Band structure of the t_{2g} three-orbital model with SOC for α-$RuCl_3$. The horizontal red dashed line indicates the Fermi level for the undoped system.

Based on the scenario that the pairing interaction arises from the PH fluctuations, we can calculate the effective electron–electron interactions using the RPA. However, as a result of the effect of the SOC, the effective particle–particle interaction cannot be simply divided into bubble and ladder diagrams as is the case with SU(2) symmetry.[50] Thus, to include the SOC in the RPA approach, we use the Hugenholtz diagrams in our calculations.[20] In this method, the susceptibilities from the PH excitations are given by

$$\widehat{\chi}(q) = \widehat{\chi}^0(q)\left[\widehat{1} + \widehat{\Gamma}\widehat{\chi}^0(q)\right]^{-1}, \tag{3}$$

where $\widehat{\Gamma}$ is the Hugenholtz bare vertex[20] and $\widehat{1}$ is the identity matrix. The non-interacting susceptibility is given by

$$\chi^0_{ij,\mu\nu}(q) = -\frac{T}{N}\sum_k G^0_{i\mu}(k+q)G^0_{\nu j}(k), \tag{4}$$

with the number of unit cell N and the temperature T. The bare Green's function is written as

$$\widehat{G}^0(k) = [i\omega_n - \widehat{H}_{t_{2g}}(\boldsymbol{k}) + \mu]^{-1}. \tag{5}$$

Here, the labels i, j, μ, and ν involve all of the degrees of freedom (sublattice, orbital, and spin) in an unit cell. Thus, for the three-orbital model on the honeycomb lattice, $\widehat{G}$ is a 12×12 matrix, while $\widehat{\chi}$, $\widehat{\chi}^0$, and $\widehat{\Gamma}$ are 144×144 matrices. In the above, $k \equiv [\boldsymbol{k}, i\omega_n]$ ($q \equiv [\boldsymbol{q}, i\omega_m]$) with $\omega_n = (2n+1)\pi T$ ($\omega_m = 2m\pi T$) for fermions (bosons).

The effective interaction in the particle–particle channel is given by[20]

$$\Gamma^{eff}_{ij,\alpha\beta}(q) = \left[\frac{1}{2}\widehat{\Gamma} - \widehat{\Gamma}\widehat{\chi}(q)\widehat{\Gamma}\right]_{i\alpha,\beta j}. \tag{6}$$

The gap function is derived from the linearized superconducting gap equation, which is given by

$$\begin{aligned} & -\frac{T}{N}\sum_{q,\alpha\beta\mu\nu}\Gamma^{eff}_{ij,\alpha\beta}(q)G_{\alpha\mu}(k-q)G_{\beta\nu}(q-k)\Delta_{\mu\nu}(k-q) \\ & = \Lambda\Delta_{ij}(k). \end{aligned} \tag{7}$$

Considering that the dominant scatterings occur near the Fermi surface (FS), we can project the effective pairing interaction (Eq. (6)) and the gap equation (Eq. (7)) on the FS. In this way, the scattering amplitude of a Cooper pair from the state $(\boldsymbol{k}, -\boldsymbol{k})$ on the γ_1 FS to the state $(\boldsymbol{k}', -\boldsymbol{k}')$ on the γ_2 FS is calculated by[51–53]

$$\begin{aligned} & V_{\gamma_1\gamma_2}(\boldsymbol{k},\boldsymbol{k}') \\ & = \sum_{ij\alpha\beta}\psi^{i*}_{\gamma_1}(\boldsymbol{k})\psi^{j*}_{\gamma_1}(-\boldsymbol{k})\Gamma^{eff}_{ij,\alpha\beta}(\boldsymbol{k}-\boldsymbol{k}',0)\psi^{\alpha}_{\gamma_2}(\boldsymbol{k}')\psi^{\beta}_{\gamma_2}(-k'), \end{aligned} \tag{8}$$

where $\psi^i_{\gamma_1}(\boldsymbol{k})$ is the γ_1-th eigenvector of the $\widehat{H}_{t_{2g}}(\boldsymbol{k})$ matrix. We then solve the following linearized gap equation:

$$-\sum_{\gamma_2}\oint_{FS}\frac{d\boldsymbol{k}'_{\parallel}}{4\pi^2 v^F_{\gamma_2}(\boldsymbol{k}')}V_{\gamma_1\gamma_2}(\boldsymbol{k},\boldsymbol{k}')\Delta_{\gamma_2}(\boldsymbol{k}') = \Lambda\Delta_{\gamma_1}(\boldsymbol{k}), \tag{9}$$

where $v^F_{\gamma_2}(\boldsymbol{k}')$ is the Fermi velocity for band γ_2 and $\Delta_{\gamma_1}(\boldsymbol{k})$ represents the normalized gap function along the FS γ_1. The integration and summation in Eq. (9) are along various FS patches. Here, the temperature is set at $T = 0.001$ eV and the calculation of the susceptibility is done with uniform 64×64 meshes in the momentum space. This equation can be solved as an eigenvalue problem, where the eigenvector corresponding to the largest eigenvalue Λ determines the favourable pairing symmetry.

3. Results and discussion

Let us first study the main properties of the PH excitations in the hole doped system. To find the dominant PH excitations, we classify various PH channels according to the total angular momentum of a PH pair. Generally, the susceptibility can be written in terms of $\widehat{F}_{\alpha\beta} = d^\dagger_\alpha d_\beta$; i.e., $\chi_{\mu\nu,\alpha\beta} = \langle\widehat{F}_{\nu\mu}\widehat{F}_{\alpha\beta}\rangle$. To show the labels of the effective angular momentums explicitly, we can express the annihilation operator of electrons

as $d_{\zeta jm}$, where j and m indicate the quantum numbers of the total effective angular momentum and its z component, respectively, ζ contains other quantum numbers except the angular momentum. Then, the PH excitation operators are written as $\widehat{F}^{\zeta_1\zeta_2}_{j_1m_1,j_2m_2} = d^{\dagger}_{\zeta_1 j_1 m_1} d_{\zeta_2 j_2 m_2}$, which are tensor operators. Since the representations of $d^{\dagger}_{\zeta jm}$ and $d_{\zeta jm}$ are $D^{1/2}\oplus D^{3/2}$ in the sector of effective angular momentum, the operator $\widehat{F}^{\zeta_1\zeta_2}_{j_1m_1,j_2m_2}$ has the following decomposition in the sector of effective angular momentum:

$$\begin{aligned}\widehat{F}^{\zeta_1\zeta_2}_{j_1m_1,j_2m_2} &\in (D^{1/2}\oplus D^{3/2})\otimes(D^{1/2}\oplus D^{3/2})\\ &= 2D^0\oplus 4D^1\oplus 3D^2\oplus D^3. \end{aligned} \tag{10}$$

Thus, the operator $\widehat{F}$ could be divided into irreducible tensor operators $\widehat{T}^{j_1j_2}_{jm}(\zeta_1\zeta_2)$ as given in Appendix A. Here, j_1 and j_2 are the angular momenta of the particle and hole. Therefore, including the sublattice indices on the honeycomb lattice, the susceptibilities χ are split into 144×144 channels which include $j_{\rm eff}=1/2$ excitations, $j_{\rm eff}=3/2$ excitations, and various spin–orbit excitations between the $j_{\rm eff}=1/2$ and $j_{\rm eff}=3/2$ states. Among these channels, we find numerically that the $j_{\rm eff}=1/2$ pseudospin fluctuations $S^{\eta_1\eta_2}(\boldsymbol{q})$ are dominant in the doping regime that we consider in the following discussions. The $j_{\rm eff}=1/2$ pseudospin susceptibilities $S^{\eta_1\eta_2}(\boldsymbol{q})$ are defined as

$$S^{\eta_1\eta_2}(\boldsymbol{q}) = \frac{T}{2N}\sum_{\ell_1\ell_2}\int_0^{\frac{1}{T}}\langle T_\tau S^{\eta_1}_{\ell_1}(\boldsymbol{q},\tau)S^{\eta_2}_{\ell_2}(-q,0)\rangle\,{\rm d}\tau, \tag{11}$$

where ℓ_1 and ℓ_2 are the sublattice indices, and the pseudospin operators S^{η}_{ℓ} are given by

$$\begin{aligned} S^x_\ell &= \frac{1}{\sqrt{2}}[-\widehat{T}^{\frac12\frac12}_{1,1}(\ell\ell)+\widehat{T}^{\frac12\frac12}_{1,-1}(\ell\ell)],\\ S^y_\ell &= \frac{\rm i}{\sqrt{2}}[\widehat{T}^{\frac12\frac12}_{1,1}(\ell\ell)+\widehat{T}^{\frac12\frac12}_{1,-1}(\ell\ell)],\\ S^z_\ell &= \widehat{T}^{\frac12\frac12}_{1,0}(\ell\ell). \end{aligned} \tag{12}$$

When the interactions are increased, the magnitudes of pseudospin fluctuations are drastically enhanced in contrast to other types of fluctuations.

In Figs. 2(a)–2(c), we show the diagonal (S^{xx}, S^{yy}, S^{zz}) and off-diagonal (S^{xy}) channels of the pseudospin susceptibilities together with the largest eigenvalue of $\widehat{\chi}$ along the Γ–M–K–Γ path for the number of electrons in primitive cell $n_{\rm e}=9.8, 9.7$, and 9.6 (in the parent compound, $n_{\rm e}=10$). It can be seen that the pseudospin $J_{\rm eff}=1/2$ susceptibilities capture nearly all features of the maximal eigenvalue of $\hat{\chi}$ and also show comparable intensities. Thus, the $j_{\rm eff}=1/2$ picture is robust in the doping range we consider here. The differences of S^{xx}, S^{yy}, and S^{zz} shown in Figs. 2(a)–2(c) are the reflections of the asymmetry of the Kitaev exchange interaction in the weak-coupling limit. Moreover, when rotating 120° clockwise along k_c-axis, the transformation of pseudospin fluctuations has a cycle rule: $(x,y,z)\to(y,z,x)$, namely, $S^{xx}\to S^{yy}, S^{yy}\to S^{zz}$, and $S^{zz}\to S^{xx}$, which is also coincident with the symmetry of the Kitaev interactions.[27] In the undoped α-$RuCl_3$, the material shows a zigzag magnetic order, which gives a peak of the susceptibilities at M point in the Brillouin zone.[14] Our results of the doped systems also show obvious peaks around the M point, which result from the zigzag magnetic fluctuations, though the static zigzag order for the undoped system ($n_{\rm e}=10$) can not be obtained in our calculations due to the divergence of the RPA susceptibility. For $n_{\rm e}=9.8$ (Fig. 2(a)), the peaks of the susceptibilities deviate from the M point. When the electron concentration is decreased, the peaks move to the M point again, meanwhile the intensities of the peaks are enhanced. In Figs. 2(d)–2(f), we present the pseudospin susceptibility $\mathcal{S}(\boldsymbol{q})=\sum_\eta S^{\eta\eta}(\boldsymbol{q})$, from which we can see more clearly the distribution of the pseudospin susceptibilities in the whole Brillouin zone.

We then study the properties of superconducting pairing by solving Eq. (9). We find that the maximal values of Λ are in the pseudospin-singlet pairing channel and are far greater than those of the pseduospin-triplet pairing states. So, we will only discuss the superconducting pairing in the singlet channel. In Figs. 2(g)–2(i), we present the real parts of the leading pairing gap functions for three different electron concentrations, which show basically a d-wave symmetry. To understand the detail forms of the pairing gap functions, we try to fit the gap functions by including the electron pairings up to the third nearest-neighbor sites in real space. The fitting functions are given by

$$\Delta_n(\boldsymbol{k}) = \Delta_1 d^{(1)}_{x^2-y^2}(\boldsymbol{k})+\Delta_2 d^{(2)}_{x^2-y^2}(\boldsymbol{k})+\Delta_3 d^{(3)}_{x^2-y^2}(\boldsymbol{k}), \tag{13}$$

with

$$\begin{aligned} d^{(1)}_{x^2-y^2}(\boldsymbol{k}) &= \cos(k_a/\sqrt{3})-\cos(k_a/2\sqrt{3})\cos(k_b/2),\\ d^{(2)}_{x^2-y^2}(\boldsymbol{k}) &= \cos(k_b)-\cos(\sqrt{3}/2k_a)\cos(k_b/2),\\ d^{(3)}_{x^2-y^2}(\boldsymbol{k}) &= \cos(2k_a/\sqrt{3})-\cos(k_a/\sqrt{3})\cos(k_b), \end{aligned}$$

being the first, second, and third nearest-neighbor pairing functions, respectively, and Δ_1, Δ_2, and Δ_3 being the corresponding pairing intensities. Here, n denotes the electron concentration. Using the adjustable parameters Δ_1, Δ_2, and Δ_3, we find the following optimal fitting functions for the three electron concentrations:

$$\begin{aligned} \Delta_{9.8}(\boldsymbol{k}) &= 0.11d^{(1)}_{x^2-y^2}(\boldsymbol{k})+0.55d^{(2)}_{x^2-y^2}(\boldsymbol{k})+0.83d^{(3)}_{x^2-y^2}(\boldsymbol{k}),\\ \Delta_{9.7}(\boldsymbol{k}) &= 0.96d^{(1)}_{x^2-y^2}(\boldsymbol{k})+0.07d^{(2)}_{x^2-y^2}(\boldsymbol{k})+0.26d^{(3)}_{x^2-y^2}(\boldsymbol{k}),\\ \Delta_{9.6}(\boldsymbol{k}) &= 0.80d^{(1)}_{x^2-y^2}(\boldsymbol{k})-0.56d^{(2)}_{x^2-y^2}(\boldsymbol{k})+0.22d^{(3)}_{x^2-y^2}(\boldsymbol{k}). \end{aligned} \tag{14}$$

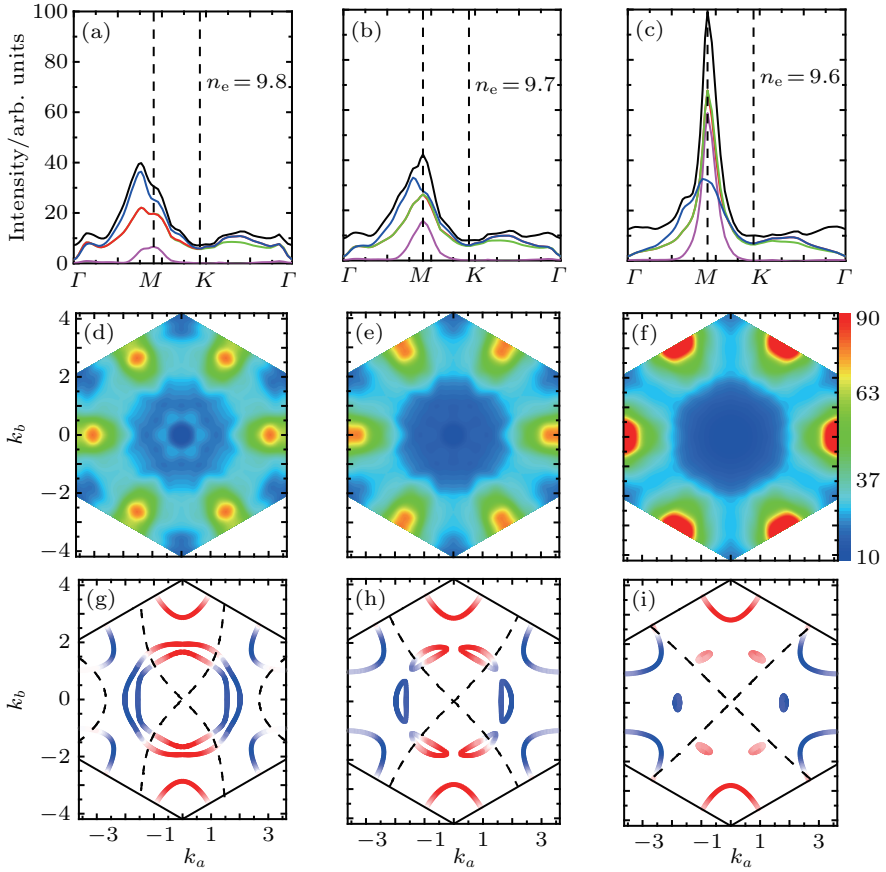


Fig. 2. Static susceptibilities and superconducting gap functions for different electron concentrations: (a), (d), (g) $n_e = 9.8$, (b), (e), (h) $n_e = 9.7$, and (c), (f), (i) $n_e = 9.6$. The up panel shows the $j_{\rm eff} = 1/2$ pseudospin susceptibilities S^{zz} (blue), S^{xx} (green), S^{yy} (red), $-S^{xy}$ (magenta), and the largest eigenvalue of $\widehat{\chi}$ defined in Eq. (3) (black) along the Γ–M–K–Γ path. Middle panel: the distribution of the sum of the pseudospin susceptibility $\sum_\eta S^{\eta\eta}(\boldsymbol{q})$ in the first Brillouin zone. Panels (g), (h), and (i) are the pairing functions for $n_e = 9.8$, $n_e = 9.7$, and $n_e = 9.6$, respectively.

Thus, the pairing gap functions for $n_e = 9.7$ and $n_e = 9.6$ have a dominant d-wave superconducting pairing along the nearest-neighbor sites, which can also been seen from the sign and nodes of the gap functions shown in Figs. 2(h) and 2(i). However, the gap function for $n_e = 9.8$ has a dominant d-wave superconducting pairing along the third-nearest-neighbor sites, so additional gap nodes appear in comparison with those for $n_e = 9.7$ and $n_e = 9.6$.

Next, we turn to the electron doped systems. In Fig. 3, we show the pseudospin susceptibility $\mathcal{S}(\boldsymbol{q})$ and superconducting gap function for $n_e = 10.1$. From Fig. 3(a), we can find that the peaks of the susceptibility are also located near M and its symmetric points. However, the intensities of the peaks are much larger than those for the hole-doped systems shown in Figs. 2(d)–2(f), which might be the origin of the persistence of the charge gap in the electron-doped systems found in the experiment,[44] i.e., the strong pseudospin fluctuations hinder the movements of the doped electrons. The superconducting gap function in Fig. 3(b) also shows a d-wave symmetry and the optimal fitting function is given by

$$\Delta_{10.1}(\boldsymbol{k}) = 0.64 d^{(1)}_{x^2-y^2}(\boldsymbol{k}) + 0.64 d^{(2)}_{x^2-y^2}(\boldsymbol{k}) + 0.21 d^{(3)}_{x^2-y^2}(\boldsymbol{k}). \quad (15)$$

We find that the electron pairing is dominated by both the nearest-neighbor and next-nearest-neighbor parings, and they have nearly the same intensity.

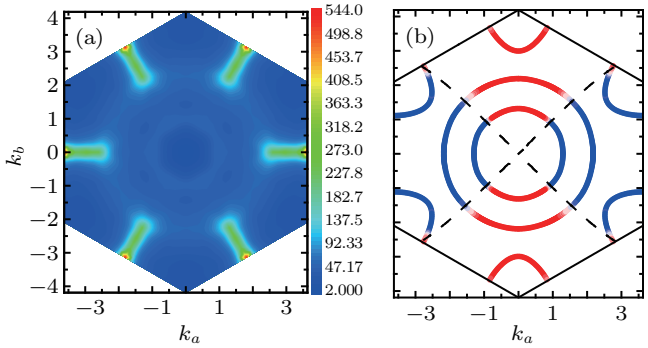


Fig. 3. (a) Static susceptibility and (b) superconducting gap function for electron doped system with $n_e = 10.1$.

Thus, we find that the d-wave pairing mediated by the $j_{\rm eff} = 1/2$ pseudospin fluctuations is the most favorable superconducting pairing symmetry for both hole and electron dopings. The explicit forms of the d-wave gap functions we obtained here are expected to be helpful for identifying the pairing symmetry if superconductivity in α-$RuCl_3$ is realized experimentally in the future.

4. Conclusion

In summary, based on the multi-band Hubbard model with all t_{2g} orbitals and by use of the random-phase approximation, we have investigated various particle–hole excitations and possible superconducting pairing symmetry in doped α-$RuCl_3$, in which the strong spin–orbit coupling and electron correlations cause an effective total angular momentum $j_{\rm eff} = 1/2$ Mott insulator. We find that the $j_{\rm eff} = 1/2$ pseudospin fluctuation dominates over other fluctuations in a large doping range, which suggests that the $j_{\rm eff} = 1/2$ picture is still robust in the doped systems. Through projecting particle–particle interaction onto Fermi surfaces, we find that the d-wave pairing is the most favorable superconducting pairing symmetry in both the hole- and electron-doped systems.

Appendix A: Decomposition of particle–hole operator

The PH operators $\widehat{F}^{\zeta_1\zeta_2}_{j_1m_1,j_2m_2} = d^{\dagger}_{\zeta_1 j_1 m_1} d_{\zeta_2 j_2 m_2}$ under rotation have the following properties:

$$\begin{aligned}\widehat{F}^{\zeta_1\zeta_2}_{j_1m_1,j_2m_2} &\to \sum_{m'_1m'_2} \widehat{F}^{\zeta_1\zeta_2}_{j_1m'_1,j_2m'_2} D^{j_1}_{m'_1,m_1}(R) D^{j_2*}_{m'_2,m_2}(R) \\ &= \sum_{m'_1m'_2} \widehat{F}^{\zeta_1\zeta_2}_{j_1m'_1,j_2m'_2} D^{j_1}_{m'_1,m_1}(R) D^{j_2}_{-m'_2,-m_2}(R) \\ &\quad \times (-1)^{2j_2-m_2-m'_2} \\ &= \sum_{jmm'm'_1m'_2} \widehat{F}^{\zeta_1\zeta_2}_{j_1m'_1,j_2m'_2} C^{j_1j_2j}_{m'_1-m'_2m} C^{j_1j_2j}_{m_1-m_2m'} \\ &\quad \times D^{j}_{m,m'}(R)(-1)^{2j_2-m_2-m'_2}. \end{aligned} \tag{A1}$$

Here, $C^{j_1j_2j}_{m_1-m_2m'}$ are the Clebsch–Gordan coefficients and $D^{j_1}_{m'_1,m_1}(R)$ is the representation of the group element R in SU(2). Thus, an irreducible representation of SU(2) is written as

$$\begin{aligned}&\widehat{T}^{j_1j_2}_{jm}(\zeta_1\zeta_2) \\ &= \sum_{m_1m_2} d^{\dagger}_{\zeta_1 j_1 m_1} d_{\zeta_2 j_2 m_2} C^{j_1j_2j}_{m_1-m_2m}(-1)^{j_2-m_2} N(jm), \end{aligned} \tag{A2}$$

where $N(jm)$ is a normalized factor. The tensor operators satisfy the relation $\widehat{T}^{\dagger j_1j_2}_{jm}(\zeta_1\zeta_2) = \widehat{T}^{j_2j_1}_{j-m}(\zeta_2\zeta_1)(-1)^{j_2-j_1+m}$. For example, the explicit formalism of $\widehat{T}^{j_1=\frac{1}{2}j_2=j_1}_{j=1,0m}(\ell_1\ell_2)$ is given by

$$\begin{aligned}\widehat{T}^{\frac{1}{2}\frac{1}{2}}_{00}(\ell_1\ell_2) &= \frac{1}{\sqrt{2}}(d^{\dagger}_{\ell_1\frac{1}{2}\frac{1}{2}} d_{\ell_2\frac{1}{2}\frac{1}{2}} + d^{\dagger}_{\ell_1\frac{1}{2}\frac{-1}{2}} d_{\ell_2\frac{1}{2}\frac{-1}{2}}), \\ \widehat{T}^{\frac{1}{2}\frac{1}{2}}_{10}(\ell_1\ell_2) &= \frac{1}{\sqrt{2}}(d^{\dagger}_{\ell_1\frac{1}{2}\frac{1}{2}} d_{\ell_2\frac{1}{2}\frac{1}{2}} - d^{\dagger}_{\ell_1\frac{1}{2}\frac{-1}{2}} d_{\ell_2\frac{1}{2}\frac{-1}{2}}), \\ \widehat{T}^{\frac{1}{2}\frac{1}{2}}_{11}(\ell_1\ell_2) &= -d^{\dagger}_{\ell_1\frac{1}{2}\frac{1}{2}} d_{\ell_2\frac{1}{2}\frac{-1}{2}}, \\ \widehat{T}^{\frac{1}{2}\frac{1}{2}}_{1-1}(\ell_1\ell_2) &= d^{\dagger}_{\ell_1\frac{1}{2}\frac{-1}{2}} d_{\ell_2\frac{1}{2}\frac{1}{2}}. \end{aligned} \tag{A3}$$

Here, the operators $d_{i,jm}$ are set by a unitary transformation

$$\begin{pmatrix} d_{i,\frac{1}{2}\frac{1}{2}} \\ d_{i,\frac{1}{2}\frac{-1}{2}} \\ d_{i,\frac{3}{2}\frac{3}{2}} \\ d_{i,\frac{3}{2}\frac{1}{2}} \\ d_{i,\frac{3}{2}\frac{-1}{2}} \\ d_{i,\frac{3}{2}\frac{-3}{2}} \end{pmatrix} = \begin{pmatrix} 0 & 0 & \frac{-1}{\sqrt{3}} & \frac{-1}{\sqrt{3}} & \frac{\mathrm{i}}{\sqrt{3}} & 0 \\ \frac{-1}{\sqrt{3}} & \frac{-\mathrm{i}}{\sqrt{3}} & 0 & 0 & 0 & \frac{1}{\sqrt{3}} \\ \frac{\mathrm{i}}{\sqrt{2}} & \frac{1}{\sqrt{2}} & 0 & 0 & 0 & 0 \\ 0 & 0 & \frac{-2\mathrm{i}}{\sqrt{6}} & \frac{\mathrm{i}}{\sqrt{6}} & \frac{1}{\sqrt{6}} & 0 \\ \frac{-\mathrm{i}}{\sqrt{6}} & \frac{1}{\sqrt{6}} & 0 & 0 & 0 & \frac{-2\mathrm{i}}{\sqrt{6}} \\ 0 & 0 & 0 & \frac{-\mathrm{i}}{\sqrt{2}} & \frac{1}{\sqrt{2}} & 0 \end{pmatrix} \begin{pmatrix} d_{i,yz\uparrow} \\ d_{i,xz\uparrow} \\ d_{i,xy\uparrow} \\ d_{i,yz\downarrow} \\ d_{i,xz\downarrow} \\ d_{i,xy\downarrow} \end{pmatrix}. \tag{A4}$$

Then, it is convenient to introduce the Hermitian operators defined as

$$\begin{aligned} S^{j_1j_2}_{jm,1}(\ell_1\ell_2) &= \frac{1}{\sqrt{2}}(\widehat{T}^{j_1j_2}_{jm}(\ell_1\ell_2) + \widehat{T}^{\dagger j_1j_2}_{jm}(\ell_1\ell_2)), \\ S^{j_1j_2}_{jm,2}(\ell_1\ell_2) &= \frac{\mathrm{i}}{\sqrt{2}}(\widehat{T}^{j_1j_2}_{jm}(\ell_1\ell_2) - \widehat{T}^{\dagger j_1j_2}_{jm}(\ell_1\ell_2)), \end{aligned} \tag{A5}$$

with $m \le 0$. Especially, for $m = 0$ and $\ell_1 = \ell_2$, the operator $S^{j_1j_2}_{jm,0} = \widehat{T}^{j_1j_2}_{jm}(\ell_1\ell_2)$ is real. Under condition $j = 1$, $\ell_1 = \ell_2$, and $j_1 = j_2$, the Hermitian operators are spin operators such as $S^{\alpha}_{\ell_1}(\alpha = x, y, z)$. With these operators, the susceptibility $\widehat{\chi}(q)$ is divided into 144×144 channels which include AB sublattice fluctuations and the different angular momentum j fluctuations.

References

[1] Lee P A, Nagaosa N and Wen X G 2006 *Rev. Mod. Phys.* **78** 17
[2] Imada M, Fujimori A and Tokura Y 1998 *Rev. Mod. Phys.* **70** 1039
[3] Stewart G R 2011 *Rev. Mod. Phys.* **83** 1589
[4] Damascelli A, Hussain A and Shen Z X 2003 *Rev. Mod. Phys.* **75** 473
[5] Xiang T and Xue J 2017 *Physics* **46** 514
[6] Luo X G, Wu T and Chen X H 2017 *Physics* **46** 499
[7] Kim B J, Jin H, Moon S J, Kim J Y, Park B G, Leem C S, Yu J, Noh T W, Kim C, Oh S J, Park J H, Durairaj V, Cao G and Rotenberg E 2008 *Phys. Rev. Lett.* **101** 076402
[8] Kim B J, Ohsumi H, Komesu T, Sakai S, Morita T, Takagi H and Arima T 2009 *Science* **323** 1329
[9] Singh Y and Gegenwart P 2010 *Phys. Rev. B* **82** 064412
[10] Liu X, Berlijn T, Yin W G, Ku W, Tsvelik A, Kim Y J, Gretarsson H, Singh Y, Gegenwart P and Hill J P 2011 *Phys. Rev. B* **83** 220403(R)
[11] Choi S K, Coldea R, Kolmogorov A N, Lancaster T, Mazin I I, Blundell S J, Radaelli P G, Singh Y, Gegenwart P, Choi K R, Cheong SW, Baker P J, Stock C and Taylor J 2012 *Phys. Rev. Lett.* **108** 127204
[12] Banerjee A, Bridges C A, Yan J Q, Aczel A A, Li L, Stone M B, Granroth G E, Lumsden M D, Yiu Y, Knolle J, Bhattacharjee S, Kovrizhin D L, Moessner R, Tennant D A, Mandrus D G and Nagler S E 2016 *Nat. Mater.* **15** 733
[13] Banerjee A, Yan J, Knolle J, Bridges C A, Stone M B, Lumsden M D, Mandrus D G, Tennant D A, Moessner R and Nagler S E 2017 *Science* **356** 1055
[14] Ran K, Wang J, Wang W, Dong Z Y, Ren X, Bao S, Li S, Ma Z, Gan Y, Zhang Y, Park J, Deng G, Danilkin S, Yu S L, Li J X and Wen J 2017 *Phys. Rev. Lett.* **118** 107203
[15] Cao G, Bolivar J, McCall S, Crow J E and Guertin R P 1998 *Phys. Rev. B* **57** 11039
[16] Kim J, Casa D, Upton M H, Gog T, Kim Y J, Mitchell J F, van Veenendaal M, Daghofer M, van den Brink J, Khaliullin G and Kim B J 2012 *Phys. Rev. Lett.* **108** 177003
[17] Ye F, Chi S, Chakoumakos B C, Fernandez-Baca J A, Qi T and Cao G 2013 *Phys. Rev. B* **87** 140406
[18] Kim Y K, Krupin O, Denlinger J D, Bostwick A, Rotenberg E, Zhao Q, Mitchell J F, Allen J W and Kim B J 2014 *Science* **345** 187
[19] de la Torre A, Walker S M, Bruno F, Riccó S, Wang Z, Lezama I G, Scheerer G, Giriat G, Jaccard D, Berthod C, Kim T, Hoesch M, Hunter E, Perry R, Tamai A and Baumberger F 2015 *Phys. Rev. Lett.* **115** 176402
[20] Wang H, Yu S L and Li J X 2015 *Phys. Rev. B* **91** 165138

[21] Cao Y, Wang Q, Waugh J A, Reber T J, Li H, Zhou X, Parham S, Park S R, Plumb N C, Rotenberg E, Bostwick A, Denlinger J D, Qi T, Hermele M A, Cao G and Dessau D S 2016 *Nat. Commun.* **7** 11367

[22] Wang F and Senthil T 2011 *Phys. Rev. Lett.* **106** 136402

[23] Watanabe H, Shirakawa T and Yunoki S 2013 *Phys. Rev. Lett.* **110** 027002

[24] Meng Z Y, Kim Y B and Kee H Y 2014 *Phys. Rev. Lett.* **113** 177003

[25] Kim Y K, Sung N H, Denlinger J D and Kim B J 2015 *Nat. Phys.* **12** 37

[26] Yan Y J, Ren M Q, Xu H C, Xie B P, Tao R, Choi H Y, Lee N, Choi Y J, Zhang T and Feng D L 2015 *Phys. Rev. X* **5** 041018

[27] Kitaev A 2006 *Ann. Phys.* **321** 2

[28] Jackeli G and Khaliullin G 2009 *Phys. Rev. Lett.* **102** 017205

[29] Winter S M, Li Y, Jeschke H O and Valentí R 2016 *Phys. Rev. B* **93** 214431

[30] Wang W, Dong Z Y, Yu S L and Li J X 2017 *Phys. Rev. B* **96** 115103

[31] Zheng J, Ran K, Li T, Wang J, Wang P, Liu B, Liu Z X, Normand B, Wen J and Yu W 2017 *Phys. Rev. Lett.* **119** 227208

[32] Yu Y J, Xu Y, Ran K J, Ni J M, Huang Y Y, Wang J H, Wen J S and Li S Y 2018 *Phys. Rev. Lett.* **120** 067202

[33] Banerjee A, Lampen-Kelley P, Knolle J, Balz C, Aczel A A, Winn B, Liu Y, Pajerowski D, Yan J, Bridges C A, Savici A T, Chakoumakos B C, Lumsden M D, Tennant D A, Moessner R, Mandrus D G and Nagler S E 2018 *NPJ Quantum Materials* **3** 8

[34] Cui Y, Zheng J, Ran K, Wen J, Liu Z X, Liu B, Guo W and Yu W 2017 *Phys. Rev. B* **96** 205147

[35] Wang Z, Guo J, Tafti F F, Hegg A, Sen S, Sidorov V A, Wang L, Cai S, Yi W, Zhou Y, Wang H, Zhang S, Yang K, Li A, Li X, Li Y, Liu J, Shi Y, Ku W, Wu Q, Cava R J and Sun L 2018 *Phys. Rev. B* **97** 245149

[36] Bastien G, Garbarino G, Yadav R, Martinez-Casado F J, Beltrán Rodríguez R, Stahl Q, Kusch M, Limandri S P, Ray R, Lampen-Kelley P, Mandrus D G, Nagler S E, Roslova M, Isaeva A, Doert T, Hozoi L, Wolter A U B, Büchner B, Geck J and van den Brink J 2018 *Phys. Rev. B* **97** 241108

[37] You Y Z, Kimchi I and Vishwanath A 2012 *Phys. Rev. B* **86** 085145

[38] Hyart T, Wright A R, Khaliullin G and Rosenow B 2012 *Phys. Rev. B* **85** 140510

[39] Okamoto S 2013 *Phys. Rev. B* **87** 064508

[40] Scherer D D, Scherer M M, Khaliullin G, Honerkamp C and Rosenow B 2014 *Phys. Rev. B* **90** 045135

[41] Schmidt J, Scherer D D and Black-Schaffer A M 2018 *Phys. Rev. B* **97** 014504

[42] Comin R, Levy G, Ludbrook B, Zhu Z H, Veenstra C N, Rosen J A, Singh Y, Gegenwart P, Stricker D, Hancock J N, van der Marel D, Elfimov I S and Damascelli A 2012 *Phys. Rev. Lett.* **109** 266406

[43] Koitzsch A, Habenicht C, Müller E, Knupfer M, Büchner B, Kandpal H C, van den Brink J, Nowak D, Isaeva A and Doert T 2016 *Phys. Rev. Lett.* **117** 126403

[44] Zhou X, Li H, Waugh J A, Parham S, Kim H S, Sears J A, Gomes A, Kee H Y, Kim Y J and Dessau D S 2016 *Phys. Rev. B* **94** 161106

[45] Koitzsch A, Habenicht C, Müller C, Knupfer M, Buchner B, Kretschmer S, Richter M, van den Brink J, Börrnert F, Nowak D, Isaeva A and Doert T 2017 *Phys. Rev. Materials* **1** 052001

[46] Sinn S, Kim C H, Kim B H, Lee K D, Won C J, Oh J S, Han M, Chang Y J, Hur N, Sato H, Park B G, Kim C, Kim H D and Noh T W 2016 *Sci. Rep.* **6** 39544

[47] Trousselet F, Horsch P, Oleś A M and You W L 2014 *Phys. Rev. B* **90** 024404

[48] Trousselet F, Berciu M, Oleś A M and Horsch P 2013 *Phys. Rev. Lett.* **111** 037205

[49] Wang B B, Wang W, Yu S L and Li J X 2015 *J. Phys.: Condens. Matter* **30** 385602

[50] Yu S L and Li J X 2013 *Chin. Phys. B* **22** 087411

[51] Graser S, Maier T A, Hirschfeld P J and Scalapino D J 2009 *New J. Phys.* **11** 025016

[52] Yu S L, Yao Z J and Li J X 2015 *J. Phys.: Condensed Matter* **27** 505701

[53] Xiao L Y, Yu S L, Wang W, Yao Z J and Li J X 2016 *Europhys. Lett.* **115** 27008